Corrosion Science 89 (2014) 154–162

Contents lists available at ScienceDirect

Corrosion Science

journal homepage: www.elsevier.com/locate/corsci

Interpretation of the relation between ferrite fraction and pitting corrosion resistance of commercial 2205 duplex stainless steel

Heon-Young Ha [a,*], Min-Ho Jang [a,b], Tae-Ho Lee [a], Joonoh Moon [a]

[a] Ferrous Alloy Department, Advanced Metallic Materials Division, Korea Institute of Materials Science, 797 Changwondaero, Seongsangu, Changwon, Gyeongnam 642-831, Republic of Korea
[b] Division of Materials Science and Engineering, Hanyang University, Seongdong-ku, Seoul 133-791, Republic of Korea

ARTICLE INFO

Article history:
Received 31 May 2014
Accepted 16 August 2014
Available online 29 August 2014

Keywords:
A. Stainless steel
B. Polarization
C. Acid corrosion
C. Pitting corrosion

ABSTRACT

The relation among pitting corrosion resistance, galvanic corrosion rate and phase fraction (44–63 vol% of ferrite phase) of UNS S32205/S31803 duplex stainless steel was investigated. The highest pitting potential was observed in the sample comprising 57 vol% of ferrite, and it decreased with increase in the phase imbalance. In the sample with 57 vol% ferrite fraction, the lowest galvanic corrosion rate between the ferrite and austenite phases was observed. It was found that the pitting corrosion resistance of the alloy samples comprising various ferrite fractions was primarily determined by the galvanic corrosion resistance between the two constituent phases.

1. Introduction

Duplex stainless steel (DSS) is a family of stainless steels consisting of approximately equal volume of ferrite (α) and austenite (γ) phases [1–5]. It is known that the DSS exhibits well-balanced characteristics of favorable mechanical strength of the α phase and the high corrosion resistance of the γ phase [6]. Furthermore, the desirable properties can be attained at relatively lower cost than the commercial FeCrNi-based austenitic stainless steels [7]. Thus, demands for the DSSs have been continuously increased in various industrial fields such as marine construction, desalination and chemical industries [1–6].

The mechanical and corrosion properties of DSSs are directly related to the microstructure, particularly the phase balance which results in the partition of alloying elements [3,6,8–10]. On various DSSs, many efforts have been made to find the optimum phase balance for the highest resistance against pitting corrosion [5,6,9,11–13]. Garfias-Mesias et al. [9] investigated the pitting corrosion resistance of UNS S32550 (26Cr–5.9Ni–3.2Mo–1.0Mn–0.2 N–1.6Cu–$Fe_{balance}$) alloy consisting of 47–64 vol% of α phase by measuring critical pitting temperature (CPT) and pitting potential (E_{pit}), and they concluded that the resistance to the pitting corrosion gradually decreased as increase in the α fraction. Hwang and Park [6] measured the pitting corrosion resistance levels of 26.2Cr–6.99Ni–2.37Mo–2.88 W–0.35 N–$Fe_{balance}$ DSS whose α fraction was controlled to be 50–53 vol%, and they reported that the samples with the α fraction of approximately 51 vol% exhibited the highest pitting corrosion resistance. Tan et al. [11] carried out the similar experiments on UNS S32750 (25.2Cr–6.7 Ni–3.4Mo–0.7Mn–0.27 N–$Fe_{balance}$) alloy whose α fraction was changed from 44 to 62 vol%. The CPT measurement on the alloy samples revealed that the sample comprising 49 vol% α fraction exhibited the highest pitting corrosion resistance. In addition, Zhang et al. [5] investigated UNS S31803 (22.4Cr–5.7Ni–3.0Mo–1.5Mn–0.17N–$Fe_{balance}$) weld metal with the α fraction of 53.6–62.5 vol%, and they reported that the highest pitting corrosion resistance was observed in the weld metal comprising 53.6 vol% of α phase. Recently, Yang et al. [12] investigated UNS S82441 (24.0Cr–3.4Ni–1.5Mo–3.0Mn–0.23 N–$Fe_{balance}$) alloy with various α fractions of 48–66 vol%. As a result, they observed that the sample with the α fraction of 48 vol% showed the highest pitting corrosion resistance, and it gradually decreased as the α fraction increased. In these papers, it was noted that the phase fraction (α:γ) which exhibited the highest resistance to pitting corrosion was approximately 50:50, and the pitting corrosion resistance generally decreased with a rise in the phase imbalance in all the DSSs, though the investigated DSSs were different.

Also notable is that the previous reports summarized above focused on the pitting resistance equivalent numbers (PRENs) of the α and the γ phases in the DSSs ($PREN_\alpha$ and $PREN_\gamma$, respectively), to explain the relation between the resistance to pitting corrosion and the phase fraction [5,6,9,11–13]. The PREN is an empirical

* Corresponding author. Tel.: +82 55 280 3422; fax: +82 55 280 3599.
E-mail address: hyha2007@kims.re.kr (H.-Y. Ha).

http://dx.doi.org/10.1016/j.corsci.2014.08.021
0010-938X/

measure of the resistance to the pitting corrosion of stainless steels, which is useful to predict the relative pitting susceptibility. The PREN is a function of the alloying elements which influence the pitting corrosion resistance, those are Cr, Mo, W, Mn, and N. Among the elements, Cr, Mo, and W are the α phase stabilizers, and Mn and N are those for the γ phase. The α and the γ phases are enriched with their stabilizers, respectively, thus the PREN values of the two constituent phases become different. In addition, the change in the volume fractions of the constituent phases determines enrichment and/or dilution of their stabilizers. Therefore, the phase fraction, partitioning of the alloy elements, and hence the PREN value of each phase are closely correlated with each other.

Most of the researchers [5,6,11–13] explained that the overall resistance to the pitting corrosion of the investigated DSS was determined by the pitting susceptibility level of less resistant phase than the other, which was predicted by the PREN values of the two phases. In addition, the experimental evidences supported that the highest pitting corrosion resistance was achieved in the annealed sample which exhibited the lowest difference in the PREN values between the α and γ, $\Delta|PREN_\alpha\text{-}PREN_\gamma|$ were provided.

Still there are some remained questions. First, the theory that the overall resistance to pitting corrosion of DSS is governed by the less resistant phase between the α and γ is not always valid. For example, the pitting corrosion resistance level of UNS S32550 was not determined by the α phase with lower PREN than the γ [9]. Furthermore, the previous papers used different PREN formulae. The PREN for stainless steel is generally expressed as PREN = [Cr]+3.3[Mo]+*x*[N], where the [alloying element] is a concentration of the element in wt%. The *x*, the [N]'s coefficient is varied from 16 to 30. In the previous papers, it was found that 16 [9], 20 [5,11] and 30 [6,12] were used for the [N]'s coefficient. When the coefficient *x* is changed, the optimum phase ratio having the lowest $\Delta|PREN_\alpha\text{-}PREN_\gamma|$ value will be changed, and then the proposed relation between the measured pitting corrosion resistance and the expected resistance level become invalid.

Based on the brief review, it can be concluded that the relation between the phase fraction and the pitting corrosion resistance of duplex stainless steels is not clarified yet. Thus, in this paper, the pitting corrosion resistance of commercial UNS S31803 (or UNS S32205) DSS consisting of the α phase of 44–63 vol% was investigated, and the relation between the pitting corrosion resistance and the phase fraction was discussed.

2. Materials and methods

The investigated alloy was commercial DSS2205 (UNS S32205/S31803, 22.44Cr–5.99Ni–3.24Mo–0.186 N–1.38Mn–0.39Si–0.024P–0.001S–0.016C–$Fe_{balance}$, in wt%). In order to control the α:γ, the DSS2205 samples (1 cm × 1 cm × 0.2 cm) were annealed at various temperatures of 1050, 1090, 1130, 1165 and 1195 °C for 1 h and quenched in water. The annealing temperatures were selected based on the equilibrium phase diagram shown in Fig. 1, which was calculated using Thermo-Calc. (version 3.0, TCFE 7 database) commercial software.

The microstructures and chemical compositions of the α and γ phases in the annealed samples were investigated using a light optical microscope (EPIPHOT, Nikon), scanning electron microscope (SEM, NanoSEM 230, FEI and JSM-7001F) equipped with an electron backscatter diffraction (EBSD, HKL Nordlys Channel 5) attachment, and an electron probe micro analysis with a wavelength dispersive spectrometry (EPMA-WDS, SX100, CAMECA). For the microscopic analysis, the annealed samples were mechanically ground on SiC emery paper and polished using a diamond suspension to 1 μm, and then electrochemically etched in KOH solution (80 g KOH in 100 ml deionized water) at 25 °C by applying

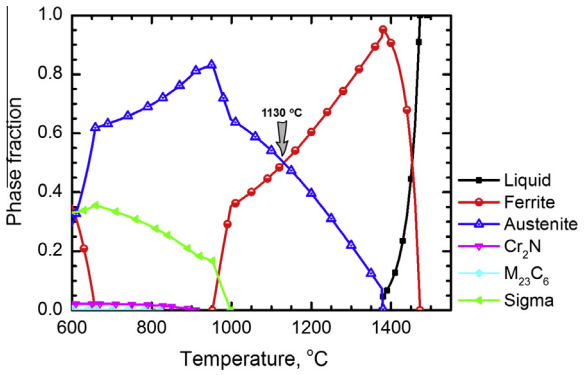

Fig. 1. Equilibrium phase diagram of the DSS2205 alloy calculated using Thermo-Calc (version 3.0, TCFE 7 database) commercial software.

4.5 V for 20–40 s. The α:γ was quantitatively analyzed on the optical micrographs using an image analyzer. The average grain sizes of the samples measured from EBSD analysis were identified with the critical misorientation angle of 5°. For the EBSD analysis, the samples were electropolished for 20 s in a mixed solution of 10 mass% perchloric acid and 90 mass% methanol at −20 °C by applying 25 V. In addition, partitioning of alloying elements in the α and γ phases of each annealed samples were examined using an EPMA.

Pitting corrosion resistance of the annealed samples was investigated using potentiodynamic polarization tests in 4 M NaCl and 3.5 M KCl solutions at 70 °C at a scan rate of 1 mV s^{-1}. For the tests, a conventional three-electrode cell of 1 L comprising a working electrode (sample), a saturated calomel reference electrode (SCE) and a Pt plate counter electrode was used, and the tests were conducted using a potentiostat (Reference 600, GAMRY). For the working electrode, the annealed specimens were mounted in cold epoxy resin, and then mechanically ground using SiC papers up to 2000 grit and washed using distilled water. The polarization tests were conducted on the exposed area of 0.13 cm^2, which was controlled using electroplating tape. The resistance to the pitting corrosion of the samples was evaluated by the E_{pit} levels measured from the polarization curves. The E_{pit} was determined as the potential at which a stable pitting corrosion occurs, that is, the potential point where a permanent increase in the anodic current density from the passive current density level is observed [14]. The initiation site for the pitting corrosion was observed using the SEM. For this, the alloy samples were polished to 1 μm using a diamond suspension, and potentiostatic tests was conducted on the samples (exposed area = 0.13 cm^2) in 4 M NaCl + 0.001 M HCl solution at 60 °C under applying 0 V_{SCE}. The acidified chloride solution rather than the neutral chloride solution was used to make it possible to observe the phase boundary and the initiation sites for the pitting corrosion simultaneously. Then, the resistance to galvanic corrosion between the α and γ phases in each annealed sample was investigated. For this, the mounted samples polished to 1 μm were immersed in 4 M NaCl + 0.01 M HCl at 60 °C for 7 h. After the immersion test, corroded topography and three-dimensional roughness were investigated using the SEM and a surface optical profiler (Wyko NT8000, Veeco [15]). The polarization tests and the immersion test were conducted at least five times and three times, respectively, and good reproducibility was confirmed.

3. Results

3.1. Microstructure

Fig. 2(a)–(e) show microstructures of the DSS2205 samples annealed at 1050–1195 °C for 1 h, respectively, which were observed using a light optical microscope. The light optical micro-

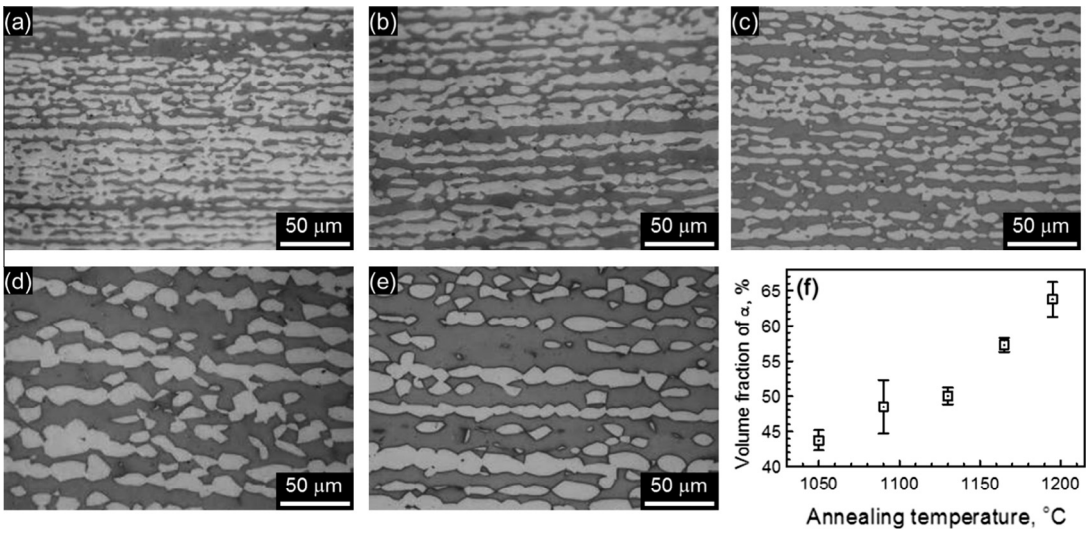

Fig. 2. Light optical micrographs of the DSS2205 samples annealed at (a) 1050 °C, (b) 1090 °C, (c) 1130 °C, (d) 1165 °C, and (e) 1195 °C. (f) Change in the volume fraction of the α phase as a function of the annealing temperature. The phase fraction was quantified by image analyzer. The average and the standard deviation values (scatter band) of the α fraction were obtained from 5 analyses results.

graphs (Fig. 2) present the relatively dark α phase and bright γ phase in banded structure along the rolling direction. From SEM images taken at a low magnification (Fig. 3(a)–(c)), it is confirmed that the nonmetallic inclusion containing S was not observed due to the extremely low S content of this alloy. Instead, only a few inclusions were observed, which were revealed to be (Mn, Cr)-oxides, and the numbers and distribution of the inclusions were similar in all the annealed samples. In addition, the SEM images taken at a high magnification (Fig. 3(a′)–(c′)) show that carbides and/or nitrides were not precipitated during the annealing.

As the annealing temperature was elevated, the α fraction and the average grain size increased. The phase fraction was quantified by image analyzing on the representative 5 optical micrographs. As a result, the volume fraction of the α phase linearly increased from 44 to 63 vol% with the rise in the annealing temperature from 1050 to 1195 °C as shown in Table 1 and Fig. 2(f). The EBSD analysis was employed to measure the average grain sizes of the samples. In the EBSD maps in Fig. 4, the yellow- and red-colored phases were the α and the γ, respectively (Fig. 4(f)). The grain sizes of the α and the γ phases of the alloy samples annealed at 1050 °C were 4.39 and 4.19 μm, and those of the sample annealed at 1195 °C were 7.25 and 5.90 μm, respectively. These results showed a good agreement with the previous reports [6,11].

3.2. Alloy element partitioning

For each sample, 10–12 points were analyzed using an EPMA, and the average compositions of the alloying elements (Cr, Mo, Ni, Mn, N and C) in the α and the γ phases are presented in Table 1. In addition, Fig. 5(a)–(e) present the variations of the chemical compositions of Cr, Mo, Ni, Mn and N of the α and the γ phases as a function of the α fraction, respectively. It was confirmed that the α phase contained the higher content of Cr and Mo (Fig. 5(a) and (b), respectively), and the γ phase had the larger amount of Ni, Mn and N (Fig. 5(c)–(e), respectively) [5,10–12,16]. Regarding C, because C is a strong γ stabilizer, the C content of the γ phase was higher than that of the α phase. The C content of the γ phase gradually increased from 0.023 to 0.031 wt% as the α fraction

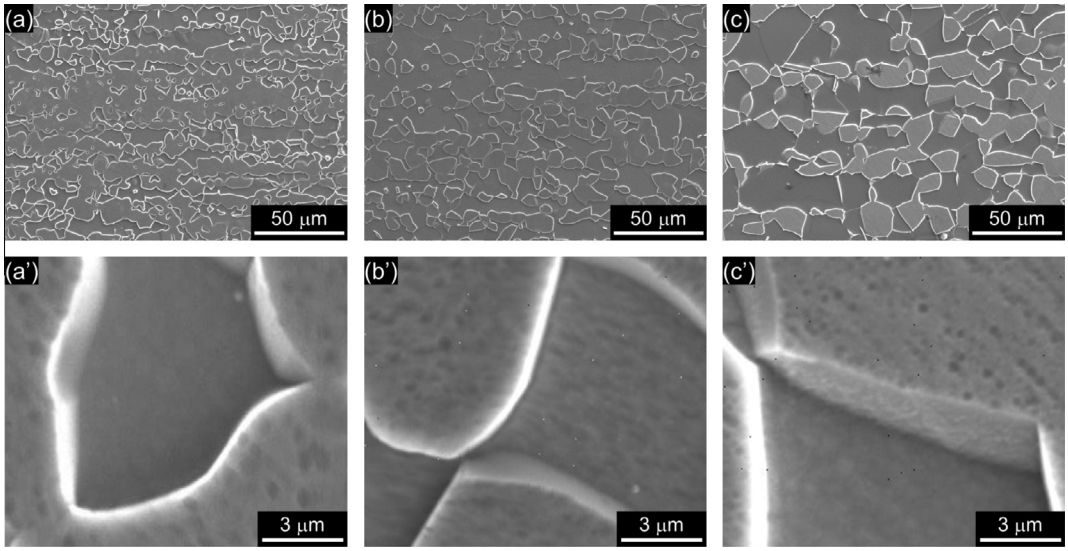

Fig. 3. SEM micrographs of the DSS2205 samples annealed at (a) 1050 °C, (b) 1130 °C, and (c) 1195 °C taken at (a)–(c) low and (a′)–(c′) high magnifications.

Table 1
Annealing temperatures, volume fractions of α phase, chemical compositions and the PREN values of the α and γ phases of the DSS2205 annealed samples. The average and the standard deviation values of the chemical composition were obtained from 10 to 12 measurement results.

Annealing temperature (°C)	Volume fraction of α (%)	Phase	Composition, average ± standard deviation (wt%)						$PREN_{\alpha}$*	$PREN_{\gamma-16}$**	$PREN_{\gamma-30}$***
			Cr	Mo	Ni	Mn	N	C			
1050	44	α	24.485 ± 0.412	4.399 ± 0.163	4.653 ± 0.251	1.281 ± 0.038	0.050 ± 0.030	⩽0.01	39.0	–	–
		γ	21.253 ± 0.211	2.519 ± 0.034	7.216 ± 0.053	1.453 ± 0.081	0.261 ± 0.141	0.023 ± 0.0035	–	32.3	35.9
1090	48	α	24.087 ± 0.168	4.375 ± 0.062	4.827 ± 0.077	1.294 ± 0.073	0.067 ± 0.042	⩽0.01	38.5	–	–
		γ	21.286 ± 0.140	2.584 ± 0.039	7.220 ± 0.045	1.484 ± 0.034	0.311 ± 0.078	0.025 ± 0.0053	–	33.3	37.7
1130	50	α	23.604 ± 0.532	4.216 ± 0.059	5.003 ± 0.118	1.300 ± 0.114	0.062 ± 0.010	⩽0.01	37.5	–	–
		γ	21.501 ± 0.124	2.540 ± 0.043	7.231 ± 0.089	1.493 ± 0.043	0.313 ± 0.125	0.026 ± 0.0040	–	33.4	37.8
1165	57	α	23.731 ± 0.189	4.111 ± 0.068	4.885 ± 0.093	1.308 ± 0.043	0.044 ± 0.043	⩽0.01	37.3	–	–
		γ	21.012 ± 0.126	2.601 ± 0.040	7.112 ± 0.069	1.501 ± 0.062	0.341 ± 0.074	0.029 ± 0.0049	-	33.6	38.3
1195	63	α	23.373 ± 0.155	3.820 ± 0.046	5.132 ± 0.069	1.311 ± 0.030	0.060 ± 0.036	⩽0.01	36.0	–	–
		γ	21.418 ± 0.109	2.501 ± 0.020	7.170 ± 0.086	1.429 ± 0.035	0.364 ± 0.109	0.031 ± 0.0042	–	34.1	39.2

* **$PREN_{\alpha}$** = Cr + 3.3Mo [17].
** **$PREN_{\gamma-16}$** = Cr + 3.3Mo + **16**N–Mn [4,9,22,23].
*** **$PREN_{\gamma-30}$** = Cr + 3.3Mo + **30**N–Mn [6,13,17,20,24-27].

increased. The C content in the α phase was less than 0.01 wt%, but the accurate C content of the α phase could not be obtained because of the detection limit of our analysis equipment.

The Cr content in the α phase was 23.4–24.5 wt%, which is approximately 1.7–3.2 wt% higher than that of γ phase in the annealed DSS2205 samples. The Mo content in the α phase was 3.8–4.4 wt% and that in the γ phase was 2.5–2.6 wt%. The Cr and Mo contents in the α phase were generally lowered (i.e., diluted) as increase in the α fraction, and those in the γ phase were limited and showed little dependency on the α fraction as shown in Fig. 5(a) and (b).

Regarding the γ stabilizers, the Ni content in the γ phase was approximately 7.2 wt% which was higher than that in the α phase (4.6–5.1 wt% Ni) as shown in Table 1 and Fig. 5(c). The partitioning of Mn was also clearly observed in Table 1 and Fig. 5(d) although the overall Mn content in the DSS2205 alloy was as low as 1.38 wt%. Both the Ni and Mn contents in the γ phase slightly decreased while those in the α phase slightly increased. On the other hand, the N concentration in the γ phase was in a range of 0.261–0.364 wt%, which obviously increased with increase in the α fraction, while the N content the α phase less than 0.06 wt% showed no notable change as the α fraction increased. The solubility of N in the α phase is known to be limited to less than 0.1 wt%, preferentially 0.05 wt%, which is extremely lower than that in the γ phase [9,11,12,17–20]. In addition, due to the high diffusivity of N [17] at the elevated temperature in austenitic stainless steels (approximately 7.5×10^{-8} cm^2 s^{-1} at 1050 °C [21]), almost all the N atoms in the matrix move into the γ phase during the annealing. Thus, as the α fraction increased from 44 to 63 vol% (*i.e.* the γ fraction decreased), the N concentration in the γ phase linearly increased while that remained almost constant at approximately 0.06 wt% in the α phase (Table 1 and Fig. 5(e)).

3.3. Resistance to pitting corrosion

The resistance to the pitting corrosion of the annealed DSS2205 alloy samples was evaluated using the potentiodynamic polarization tests. In order to confirm the reproducibility, the polarization tests were performed at least in quintuplicate on each sample in two kinds of chloride solutions (4 M NaCl and 3.5 M KCl), and the representative results were presented in Fig. 6. The solution temperature was controlled to be 70 °C using a heating mantle.

In the NaCl solution (Fig. 6(a)–(f)), the corrosion potential (E_{corr}) levels of the annealed samples were approximately −0.26 V_{SCE}, and all the samples exhibited passivity at their E_{corr} levels. The passive current density ($i_{passive}$) levels of the samples were in a range of 3.4–3.6 μA cm^{-2} (at −0.1 V_{SCE}). The E_{corr} and the $i_{passive}$ levels showed no dependency on the α fraction. The effect of the α fraction was observed in the E_{pit} levels of the samples. As the α fraction increased from 44 to 57 vol%, the E_{pit} level gradually increased from 0.259 to 0.433 V_{SCE}. However, the significant decrease in the E_{pit} level to 0.265 V_{SCE} was observed in the sample with the largest α fraction of 63 vol% (Fig. 6(e)). Similar result was obtained in the 3.5 M KCl solution at 70 °C (Fig. 6(a′)–(f′)). In this condition, all the samples also showed passivity at their E_{corr} level of approximately −0.24 V_{SCE}, and the $i_{passive}$ levels of the samples were in a range of 3.7–4.0 μA cm^{-2} (at −0.1 V_{SCE}). The E_{pit} level measured in this solution increased from 0.157 V_{SCE} (44 vol% α fraction, Fig. 6(a′)) to the highest value of 0.544 V_{SCE} (57 vol% α fraction, Fig. 6(d′)), while the sample comprising 63 vol% of α phase showed the decreased E_{pit} level of 0.309 V_{SCE} (Fig. 6(e′)). The measured E_{pit} levels were plotted as a function of the α fraction in Fig. 6(f) and (f′) for each condition, respectively. The curves exhibit an inverted V-shape, and the highest E_{pit} level were measured in the sample comprising 57 vol% of α phase.

The initiation sites for the pitting corrosion were investigated. The pitting corrosion was induced by a potentiostatic test in 4 M NaCl + 0.001 M HCl solution at 60 °C under applying 0 V_{SCE}, which was in the passive potential range. Fig. 7(a)–(c) present the representative corrosion morphology of the samples comprising the α fraction of 44, 50 and 63 vol%, respectively. In all the annealed samples regardless of the α fraction, it was observed that the pitting corrosion occurred mostly at the α phase adjacent to the γ phase and propagated into the α phase. The phases shown in Fig. 7 were identified by composition analysis using the EPMA. Fig. 7 also informs that the galvanic corrosion occurs between the two phases in all the samples, and it is noted that the α phase is the less noble phase than the γ phase in the annealed DSS2205 samples.

3.4. Resistance to galvanic corrosion

The galvanic corrosion resistance between the α and γ phases was investigated using a corrosion depth measurement during the immersion test in 4 M NaCl + 0.01 M HCl solution at 60 °C for 7 h. After the test, the corrosion morphology was observed using the SEM. Fig. 8 shows that one of the phases is selectively dissolved. In this corrosive condition, the corrosion of each phase was general (or uniform) corrosion, not the pitting corrosion. In all alloy samples regardless of the α fraction, the more dissolved

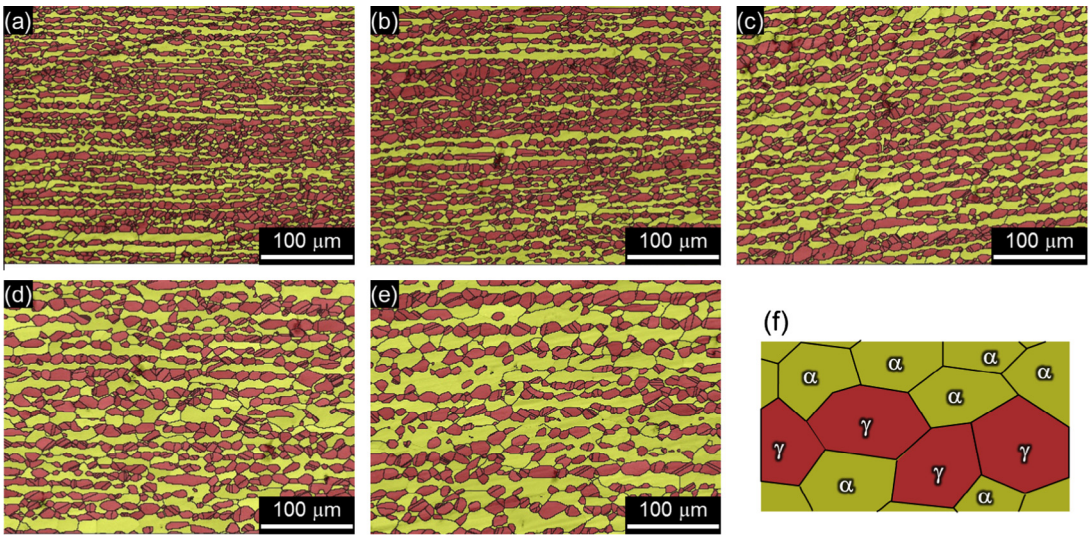

Fig. 4. EBSD phase maps of the DSS2205 samples after annealing at (a) 1050 °C, (b) 1090 °C, (c) 1130 °C, (d) 1165 °C, and (e) 1195 °C. (f) Schematic diagram of the phase map (□: body-centered cubic, α, ■: face-centered cubic, γ, ▬: misorientation angle > 5 deg).

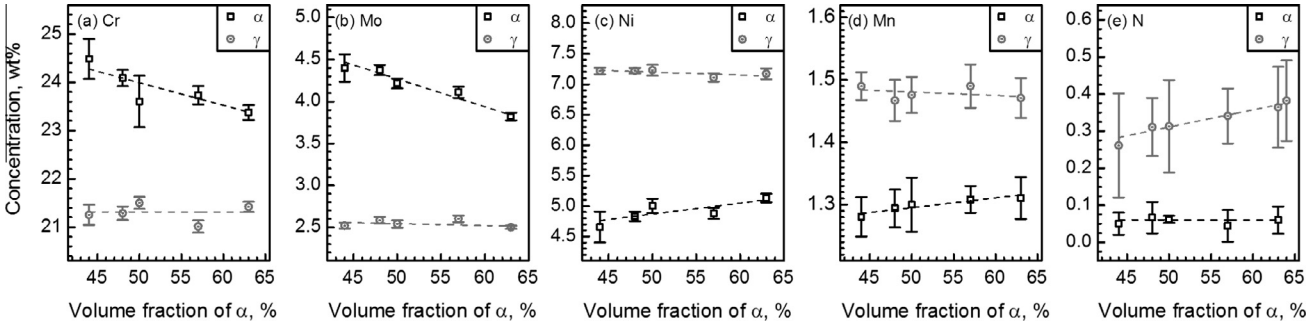

Fig. 5. Changes in the chemical compositions of (a) Cr, (b) Mo, (c) Ni, (d) Mn, and (e) N as a function of the α fraction. For each sample and each phase, 10–12 points were analyzed using an EPMA, and the average and the standard deviation values (scatter band) were presented.

phase (*i.e.*, the less noble phase) was the α phase, which was identified by composition analysis using the EPMA. The notable point in Fig. 8(a)–(e) is that the samples exhibit the difference in the corrosion depths.

The 3-dimensional shapes of corroded surfaces were investigated using the surface optical profiler, and hence the corrosion depth could be quantified from the corrosion topographs in Fig. 9. As mentioned above, the selectively corroded phase was the α phase in all the annealed samples. In addition, the corrosion depth of the α phase relative to the γ phase's surface reflected the relative corrosion rate of the α phase, i.e., the galvanic corrosion rate. Thus, the corrosion depth was plotted as a function of the α fraction in Fig. 9(f). As the α fraction increased from 44 to 57 vol%, the average corrosion depth decreased from 2.006 to 0.897 μm. However, the average corrosion depth increased to 1.362 μm in the sample comprising 63 vol% of α phase. Thus, the corrosion depth versus the α fraction showed the V-shaped curve.

4. Discussion

As discussed in the introduction section, most of the previous researchers explained the overall pitting corrosion resistance of duplex stainless steels with the PREN values of the two constituent phases. Thus, in this paper, the PREN values of the α and the γ phases of each DSS2205 sample were calculated based on the chemical composition analysis results (Table 1). The PREN for the α phase ($PREN_\alpha$) was calculating using the following formula [17];

$$PREN_\alpha = [Cr] + 3.3[Mo]. \quad (1)$$

For the γ phase, the generally accepted PREN formulae are as follows;

$$PREN_{\gamma-16} = [Cr] + 3.3[Mo] + 16[N] - [Mn] \quad (2)$$

$$PREN_{\gamma-30} = [Cr] + 3.3[Mo] + 30[N] - [Mn] \quad (3)$$

In the PREN formulae for the γ phase, the widely used [N]'s coefficients were 16 [4,9,22,23] or 30 [6,13,17,20,24–27], and thus both PREN values for the γ phase were considered in this paper. In addition, it is well-known that the solutionized Mn reduces the pitting corrosion resistance, thus the coefficient of Mn in the PREN formula is −1 [13,26]. The calculated PREN values of the α and γ phases against the α fraction are plotted in Fig. 10. As the α fraction increased, the $PREN_\alpha$ decreased linearly from 39.0 to 36.0, which was due to decrease in the Cr and Mo contents as the α fraction increased. On the other hand, the $PREN_{\gamma-16}$ and $PREN_{\gamma-30}$ gradually increased which was primarily caused by the concentrated N in the γ phase along with the α fraction. The graphs for the $PREN_\alpha$ and the $PREN_{\gamma-16}$ versus the α fraction do not intersect at any point (Fig. 10(a)), while the graphs for the $PREN_\alpha$ and the $PREN_{\gamma-30}$ versus the α fraction have an intersection point at 50.8 vol% α fraction (Fig. 10(b)).

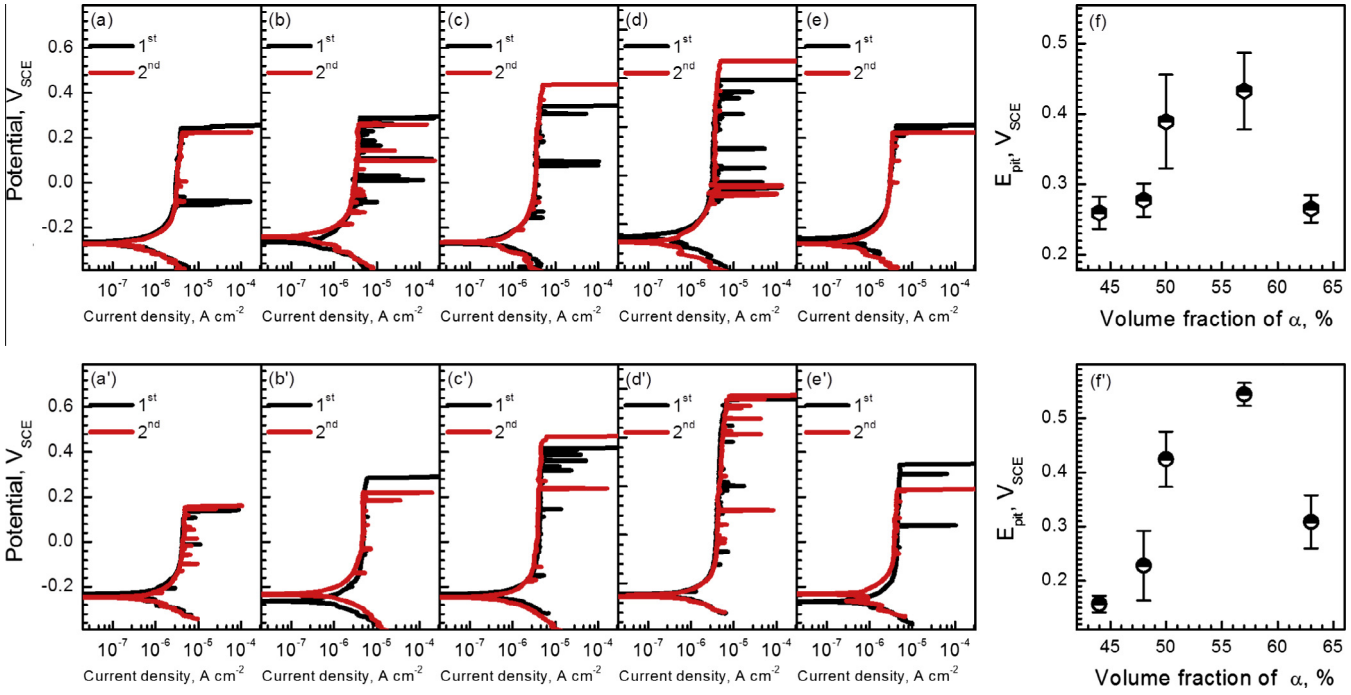

Fig. 6. Potentiodynamic polarization curves of the DSS2205 samples comprising (a)(a′) 44 vol%, (b)(b′) 48 vol%, (c)(c′) 50 vol%, (d)(d′) 57 vol%, and (e)(e′) 63 vol% measured in (a)–(e) 4 M NaCl and (a′)–(e′) 3.5 M KCl solutions at 70 °C. (f)(f′) Changes in the E_{pit} as a function of the α fraction measured in 4 M NaCl and 3.5 M KCl solutions, respectively. The average and the standard deviation values (scatter band) of the pitting potential (E_{pit}) were obtained from 5 repeated tests.

As reviewed above, it has been considered that the overall resistance to the pitting corrosion of DSSs was governed by less resistant phase against pitting corrosion having the lower PREN value than the other. If this theory is valid, the overall pitting corrosion resistance of the DSS2205 alloy can be estimated by Fig. 10. Fig. 10(a) infers that the E_{pit} levels of the annealed DSS2205 samples should gradually increase along with the α fraction, because the less resistant phase's PREN value ($PREN_{\gamma-16}$) is linearly raised. However, the practical change in the E_{pit} level along with the α fraction (Fig. 6(f) and (f′)) showed very different aspect, that is, the inverted V-shape. On the other hand, in Fig. 10(b), the two lines of PRENs versus the α fraction cross at 50.8 vol% α fraction point, and thus it seems to correspond to the graph of E_{pit} versus the α fraction (Fig. 6(f) and (f′)). However, it is difficult to conclude that a strong correlation exists between the measured pitting corrosion resistance (Fig. 6(f) and (f′)) and the change in the PREN values (Fig. 10(b)). The first disagreement is found in the α fraction point at which the highest pitting corrosion resistance is shown. The optimum α fraction for the highest pitting corrosion is estimated as 50.8 vol% by the PREN lines in Fig. 10(b), but the measured E_{pit} levels in Fig. 6(f) and (f′) shows that the best α fraction is 57 vol%. In addition, the more important point is the pitting corrosion initiation site. Based on Fig. 10(b), it is estimated that the pitting corrosion will be initiated at the γ phase in the DSS2205 samples comprising the α phase smaller than 50.7 vol%, and the preferential sites for the pitting corrosion initiation will be changed to the α phase in the samples comprising the α phase larger than 50.7 vol%. However, Fig. 7 demonstrates that the preferential pitting corrosion site is always the α phase regardless of the α fraction, even in the samples consisting of less than the 50.8 vol% of α phase. This phenomenon was also found in the literature [9,12,28]. In UNS S82441 (24Cr–3.4Ni–1.5Mo–3Mn–0.23 $N–Fe_{balance}$) alloy, the pitting corrosion preferentially occurred in the α phase regardless of change in the α fraction from 48 to 66 vol% [12]. In addition, Garfias-Mesias et al. [9] also reported that the pitting corrosion was confined to the α phase in the UNS S32550 (26Cr–5.9Ni–3.2Mo–1.0Mn–0.2 $N–1.6Cu–Fe_{balance}$) comprising 47–64 vol% of α phase. For these reasons, it is concluded that the overall pitting corrosion resistance of the annealed DSS2205 samples should not be estimated by the PREN values only.

The strong correlation was found between the change in the E_{pit} level (Fig. 6(f) and (f′)) and the corrosion depth (Fig. 9(f)) as a function of the α fraction. The DSS2205 alloy sample comprising 57 vol% of α phase exhibited the lowest galvanic corrosion resistance among the samples, in which the highest resistance against the pitting corrosion was observed. In addition, the increase in the corrosion depth was closely related to the decrease in the E_{pit} level of the samples. Furthermore, the selectively dissolved phase

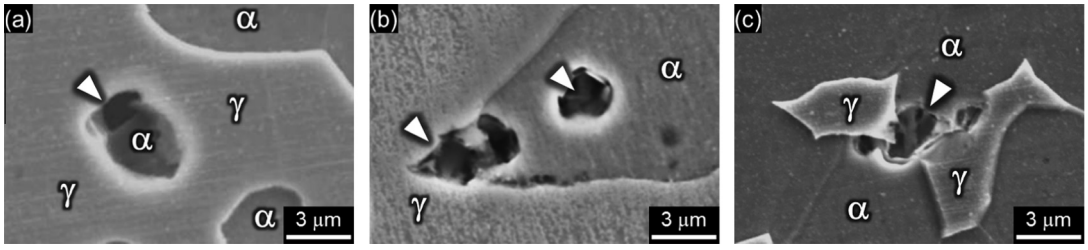

Fig. 7. SEM micrographs of pitted surfaces of the DSS2205 samples comprising (a) 44 vol%, (b) 50 vol%, and (c) 63 vol%.

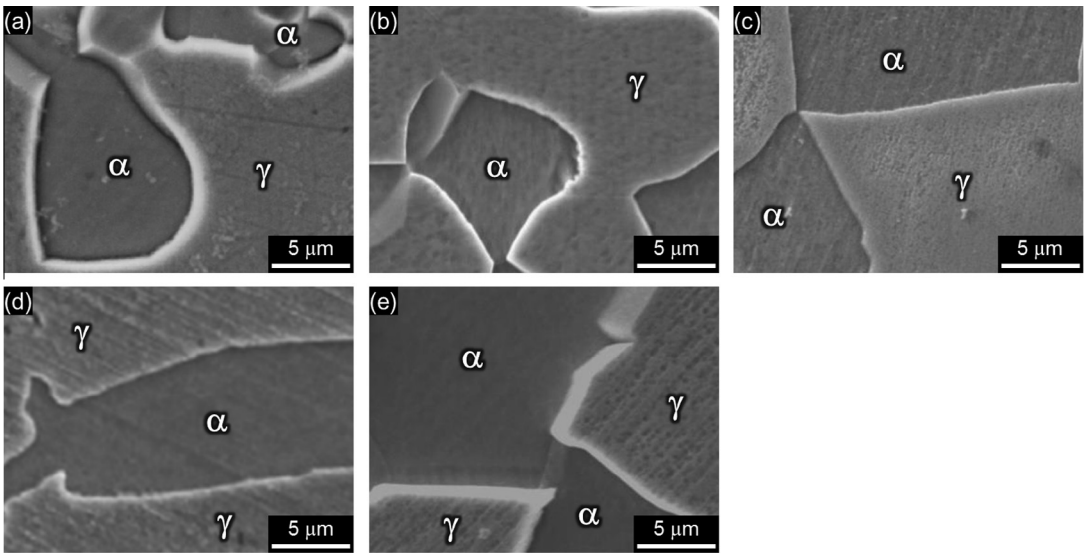

Fig. 8. SEM micrographs of galvanically corroded surfaces of the DSS2205 samples comprising (a) 44 vol%, (b) 48 vol%, (c) 50 vol%, (d) 57 vol%, and (e) 63 vol%.

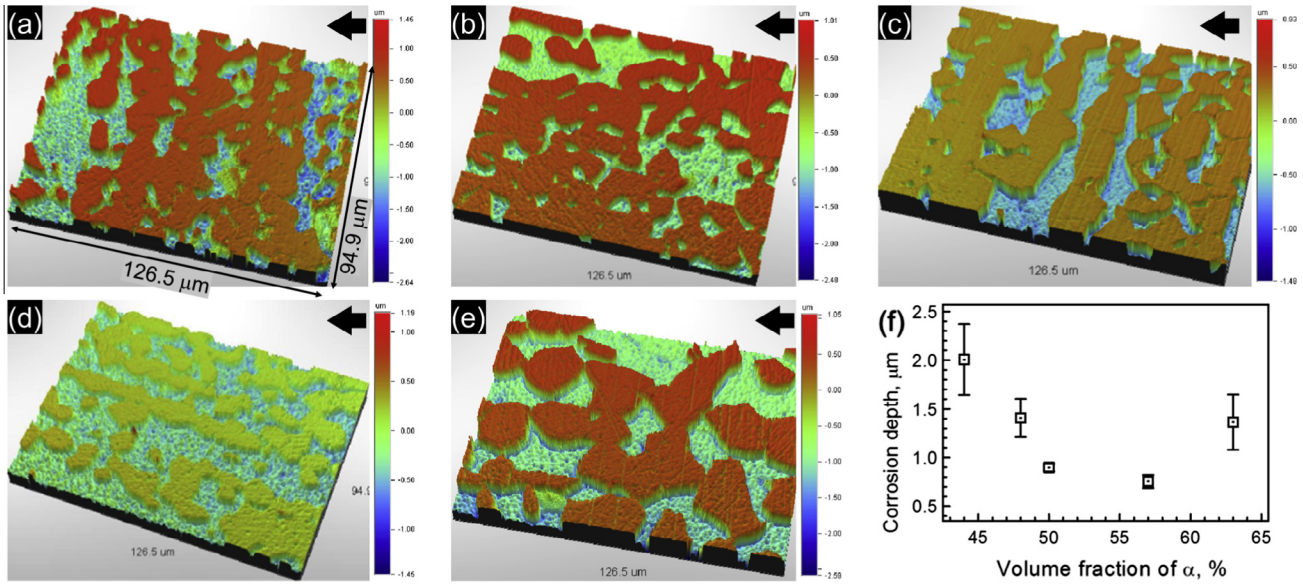

Fig. 9. 3-dimensional topographs of galvanically corroded surfaces of the DSS2205 samples comprising (a) 44 vol%, (b) 48 vol%, (c) 50 vol%, (d) 57 vol%, and (e) 63 vol%, which were investigated using a surface optical profiler. (f) Change in the corrosion depth as a function of the α fraction. The average and the standard deviation values (scatter band) of the corrosion depth were obtained from 10 to 15 measurement results.

during the immersion test is the α phase, which showed a good agreement with the observation that the pitting corrosion occurred mostly at the α phase adjacent to the γ phase, and propagated into the α phase.

The pitting corrosion phenomenon is a kind of various types of localized corrosion which is initiated by breakdown of the passive film mostly due to the chloride ion attack in aqueous solution. During the pit growth in Fe-based metals, the chloride solution inside the occluded pit become acidified due to the hydrolysis reaction [29,30]. Inside the pit, the bare surface of metal without the passive film is exposed to the acidified chloride solution, and then general corrosion of the matrix takes place. Thus the pitting propagation or growth rate is governed by the uniform dissolution rate of the matrix. The overall pitting corrosion resistance of the DSS2205 samples comprising the various α fractions is affected by the resistance to the pitting corrosion initiation and resistance to the pitting corrosion propagation as well. The former is determined by various factors, including the PREN level of each phase and the area which is susceptible to the pitting corrosion initiation (that is, the α phase fraction and the area fraction of the grain boundary). The latter is governed by the galvanic corrosion resistance in this case, that is the difference in the E_{corr} levels and the area ratio between the two phases. It is conceivable that the pit embryos are more frequently formed in the phase with less PREN value, but the growth of the pits is more activated in the samples showing the higher galvanic corrosion rate. In addition, the E_{pit} level measured from the polarization test is the potential point where the stable pit occurs. Thus, the change in the E_{pit} levels ver-

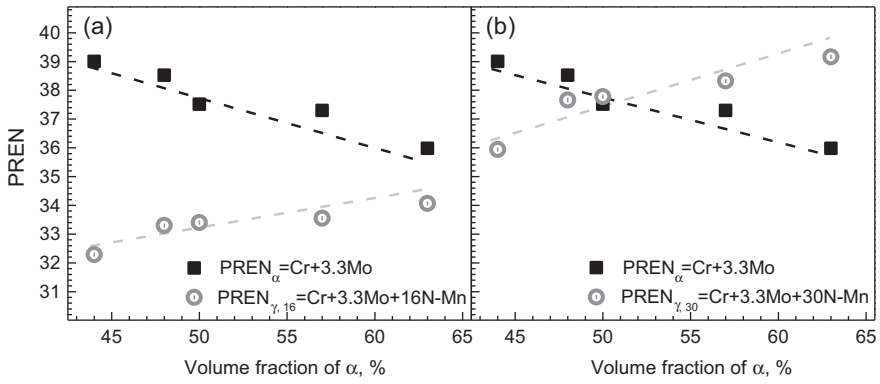

Fig. 10. Changes in the (a) $PREN_\alpha$ and $PREN_{\gamma-16}$ values and (b) $PREN_\alpha$ and $PREN_{\gamma-30}$ values as a function of the α fraction.

sus the α fraction showed stronger correlation with the change in the galvanic corrosion resistance along with the α fraction than the change in the PRENs of the two phases.

In the light of our findings, it is inferred that the balance of the E_{corr} levels between the α and the γ phases is as important as the balance in the PREN values, in design of new corrosion-resistant DSS alloy. Therefore, further works are required to find an empirical equation for the E_{corr} level which can be estimated from the alloying element like the PREN.

5. Conclusions

The relation between the pitting corrosion resistance and the phase fraction (ferrite:austenite, α:γ) was investigated on commercial duplex stainless steel, DSS2205 (UNS S32205/S31803, 22.44Cr–5.99Ni–3.24Mo–0.186 N–1.38Mn–0.39Si–0.024P–0.001S–0.016C–$Fe_{balance}$). The following four points summarize the findings of this research.

(1) The α fractions of the DSS2205 samples were controlled to be 44–63 vol% by annealing at 1050–1195 °C. The α phase was enriched with Cr and Mo, and the γ phase was enriched with Ni, Mn and N, respectively. The Cr and Mo contents in the α phase were lowered as increase in the α fraction. In addition, both the Ni and Mn contents in the γ phase slightly decreased while those in the α slightly increased. The N concentration in the γ phase obviously increased with increase in the α fraction, while that in the α showed no notable change as the α fraction increased.

(2) The resistance to the pitting corrosion of the annealed DSS2205 samples was evaluated using a potentiodynamic polarization tests. As the α fraction increased to 57 vol%, the E_{pit} level gradually increased, however, the significant decrease in the E_{pit} level was observed in the sample with the α fraction of 63 vol%. The graph of measured E_{pit} levels versus the α fraction exhibited an inverted V-shape, and the highest E_{pit} level was measured in the sample comprising 57 vol% of α phase. In all the annealed samples, the pitting corrosion occurred mostly at the α phase adjacent to the γ phase and propagated into the α phase.

(3) The galvanic corrosion resistance between the α and γ phases of the annealed samples was investigated by an immersion test and the corrosion depth was measured. It was revealed that the more dissolved phase (*i.e.*, the less noble phase) was the α phase in all the alloy samples regardless of the α fraction. The corrosion depth reflecting the galvanic corrosion rate was quantified from 3-dimensional corrosion topographs. As the α fraction increased to 57 vol%, the average corrosion depth decreased, however, in the sample comprising 63 vol% of α phase, the average corrosion depth increased. Thus, the graph of the corrosion depth versus the α fraction showed a V-shaped curve.

(4) It was revealed that the measured resistance against the pitting corrosion of the annealed DSS2205 samples comprising 44–63 vol% α fraction showed a stronger correlation with the galvanic corrosion rate between the α and γ phases than the pitting resistance equivalent numbers of the two phases which were calculated based on the chemical composition analysis results. This phenomenon inferred that the stable pitting corrosion resistance was determined by the pit growth rate rather than the pit initiation probability.

Acknowledgement

This work was supported by a grant from the Fundamental R&D Program for Core Technology of Materials funded by the Ministry of Trade, Industry & Energy, Republic of Korea.

References

[1] J. Charles, Duplex stainless steels – a review after DSS '07 held in Grado, Steel Res. Int. 79 (2008) 455–465.
[2] T. Maki, T. Furuhara, K. Tsuzaki, Microstructure development by thermomechanical processing in duplex stainless steel, ISIJ Int. 41 (2001) 571–579.
[3] J.H. Potgieter, P.A. Olubambi, L. Cornish, C.N. Machio, E.-S.M. Sherif, Influence of nickel additions on the corrosion behaviour of low nitrogen 22% Cr series duplex stainless steels, Corros. Sci. 50 (2008) 2572–2579.
[4] M. Rosso, I. Peter, D. Suani, About heat treatment and properties of duplex stainless steels, J. Achieve. Mater. Manuf. Eng. 59 (2013) 26–36.
[5] Z. Zhang, Z. Wang, Y. Jiang, H. Tan, D. Han, Y. Guo, Effect of post-weld heat treatment on microstructure evolution and pitting corrosion behavior of UNS S31803 duplex stainless steel welds, Corros. Sci. 62 (2012) 42–50.
[6] H. Hwang, Y. Park, Effects of heat treatment on the phase ratio and corrosion resistance of duplex stainless steel, Mater. Trans. 50 (2009) 1548–1552.
[7] I.-u.-H. Toor, J.H. Park, H.S. Kwon, Development of high Mn–N duplex stainless steel for automobile structural components, Corros. Sci. 50 (2008) 404–410.
[8] M.-H. Jang, J. Moon, T.-H. Lee, S.-J. Park, H.N. Han, Effect of nitrogen partitioning on Yield strength in nitrogen-alloyed duplex stainless steel during annealing, Metall. Mater. Trans. A 45 (2014) 1653–1658.
[9] L.F. Garfias-Mesias, J.M. Syke, C.D.S. Tuck, The effect of phase compositions on the pitting corrosion of 25 Cr duplex stainless steel in chloride solutions, Corros. Sci. 38 (1996) 1319–1330.
[10] L.Q. Guo, M. Li, X.L. Shi, Y. Yan, X.Y. Li, L.J. Qiao, Effect of annealing temperature on the corrosion behavior of duplex stainless steel studied by in situ techniques, Corros. Sci. 53 (2011) 3733–3741.
[11] H. Tan, Y. Jiang, B. Deng, T. Sun, J. Xu, J. Li, Effect of annealing temperature on the pitting corrosion resistance of super duplex stainless steel UNS S32750, Mater. Charact. 61 (2009) 1049–1054.
[12] Y. Yang, H. Tan, Z. Zhang, Z. Wang, Y. Jiang, J. Li, Effect of annealing temperature on the pitting corrosion behavior of UNS S82441 duplex stainless steel, Corrosion 69 (2013) 167–173.

[13] Z. Wei, J. Laizhu, H. Jincheng, S. Hongmei, Study of mechanical and corrosion properties of a Fe–21.4Cr–6Mn–1.5Ni–0.24N–0.6Mo duplex stainless steel, Mat, Sci. Eng. A-Struct. 497 (2008) 501–504.
[14] G.T. Burstein, G.O. Ilevbare, The effect of specimen size on the measured pitting potential of stainless steel, Corros. Sci. 38 (1996) 2257–2265.
[15] E. Novak, J. Schmit, White-light optical profiler with integrated primary standard, in: Damir Ilić (Ed.). Proceedings, XVII IMEKO World Congress Metrology in the 3rd Millennium June 22−27, 2003, Dubrovnik, Croatia: HMD, Croatian Metrology Soc., 2003, pp. 183–186.
[16] S. Atamert, J.E. King, Elemental partitioning and microstructural development in duplex stainless steel weld metal, Acta Metall. Mater. 39 (1991) 273–285.
[17] J.W. Simmons, Overview: high-nitrogen alloying of stainless steels, Mat. Sci. Eng. A-Struct. 207 (1996) 159–169.
[18] P.R. Levey, A. van Bennekom, A mechanistic study of the effects of nitrogen on the corrosion properties of stainless steels, Corrosion 511 (1995) 911–921.
[19] J. Rawers, G. Asai, R. Doan, J. Dunning, Mechanical and microstructural properties of nitrogen-high pressure melted Fe–Cr–Ni alloys, J. Mater. Res. 7 (1992) 1083–1092.
[20] S.-T. Kim, I.-Sy. Lee, J.-S. Kim, S.-H. Jang, Y.-S. Park, K.-T. Kim, Y.-S. Kim, Investigation of the localized corrosion associated with phase transformation of tube-to-tube sheet welds of hyper duplex stainless steel in acidified chloride environments, Corros. Sci. 64 (2012) 164–173.
[21] V.G. Gavriljuk, H. Berns, High Nitrogen Steels: Structure, Properties, Manufacture, Applications, first ed., Springer, Berlag Berlin Heidelberg, 1999.
[22] C.M.B. Martins, J.S. Moreira, J.I. Martins, Corrosion in water supply pipe stainless steel 304 and a supply line of helium in stainless steel 316, Eng. Fail. Anal. 39 (2014) 65–71.
[23] C.S. Li, T. Bell, Corrosion properties of active screen plasma nitrided 316 austenitic stainless steel, Corros. Sci. 46 (2004) 1527–1547.
[24] H. Ha, H. Kwon, Effects of Cr_2N on the pitting corrosion of high nitrogen stainless steels, Electrochim. Acta 52 (2007) 2175–2180.
[25] G. Rondelli, B. Vicentini, A. Cigada, Influence of nitrogen and manganese on localized corrosion behaviour of stainless steels in chloride environments, Mater. Corros. 46 (1995) 628–632.
[26] J.Y. Jonsson, A. Thulin, S. Hagg, R. Pettersson, The two phased optimization of duplex stainless steel, ACOM 3–4 (2013) 1–9.
[27] L. Weber, P.J. Uggowitzer, Partitioning of chromium and molybdenum in duplex stainless steels with respect to nitrogen and nickel content, Mat. Sci. Eng. A-Struct. 242 (1998) 222–229.
[28] T. Ogawa, T. Koseki, Effect of composition profiles on metallurgy and corrosion behavior of duplex stainless steel weld metals, Weld J. 68 (1989) 181s–191s.
[29] R. Newman, Pitting corrosion of metals, Electrochem. Soc. Interf. 19 (2010) 33–38.
[30] G.S. Frankel, Pitting corrosion of metals a review of the critical factors, J. Electrochem. Soc. 145 (1998) 2186–2198.